The 13th Conference on Integrated Observing and Assimilation Systems for Atmosphere, Oceans, and Land Surface, the AMS 89th Annual Meeting, 11-15 January 2009 in Phoenix, Arizona

The Application of Satellite-derived Dataset in the Analysis and Numerical Weather Prediction of the Winter Storms in Hawaii

Hsi-Chyi Yeh and Yi-Leng Chen

Department of Meteorology, University of Hawaii at Manoa

Abstract

In the subtropics, the Hawaiian Island chain surrounded by the open ocean is an excellent place to test the impact of remotely sensed data in the analysis and numerical weather prediction. In this study, the ocean surface winds derived from the QuikSCAT satellite are assimilated in the initial conditions of the regional domains over the Hawaiian Islands using WRF (Weather Research and Forecast) three-dimensional variational data assimilation system (3D-Var) for a Kona low and a cold front cases during 5-7 April and 11-13 April, 2008 respectively.

Assimilation of QuikSCAT oceanic surface winds improves the analysis of the low-level cyclonic circulation associated with the Kona low as compared with the initial conditions provided by the NCEP Global Forecast System (GFS). In addition to improved low-level circulations, the pressure field associated with the storm is also better resolved with a well defined low-pressure center at the surface. The improvement in the wind field significantly extends from the surface to the 750-hPa level. The numerical experiments with assimilating oceanic surface winds result in a relatively stronger Kona low northeast of the Hawaiian Islands.

For a cold frontal system during 11-13 April, 2008, the propagation of the surface cold front with the wind shift or wind confluence over the ocean north of the Hawaiian Islands can be captured by the analyses of QuikSCAT ocean surface winds. With the assimilated ocean surface winds, the increase of low-level east-to-northeast winds over the nearby Hawaiian Islands during the passage of the cold frontal system and the associated eastward-moving of high pressure system can be better analyzed.

1. Introduction

The Hawaiian Island chain surrounded by the open ocean is an ideal place to test the impact of remotely sensed data in the weather analysis and numerical weather prediction. In this study, the ocean surface winds derived from the QuikSCAT satellite are used to analyze the propagation of a surface cold front over the open ocean during 11-12 April 2008 and are assimilated into the initial conditions of the regional domains over the Hawaiian Islands (Fig. 1), through WRF three-dimensional variational (3D-Var) data assimilation system for a Kona storm during 5-7 April 2008. With the incorporation of the satellite-derived ocean surface winds, the improvement in the predicted sea level pressure associated with the Kona storm is investigated.

2. Data and Methodology

The QuikSCAT satellite-derived ocean surface wind data are collected twice daily and include ascending (1300-1700 UTC) and descending (0200-0400 UTC) $0.25^{o} \times 0.25^{o}$ retrieved data with blank areas over the open ocean and a daily map that covers 90% of the global ocean (Atlas et al. 2001). Frequent weather systems during the winter season in

Hawaii, including a surface cold front (11 April 2008) and a Kona storm (5 April 2008), are studied by the satellite-derived ocean surface through the low-pass objective analysis (Maddox 1980) and the Advanced Research WRF (ARW) mesoscale model (Skamarock et al. 2008) and WRF 3D-Var system (Barker et al. 2004).

3. Results

.Detection in the propagation of a surface cold front

During 11-12 April 2008, the surface weather maps show a surface front (Fig. 2) over the open ocean and propagate through the Hawaii domain. The satellite-derived ocean surface winds clearly reveal a frontal boundary (Fig. 3) where the wind shift and wind confluence are significant. The anticyclonic circulation in the prefrontal and postfrontal regions (Fig. 3) also coincides with the high-pressure systems shown on the surface map (Fig. 1a).

In addition, the propagation of the surface cold front also can be analyzed through the time series of the reanalyzed oceanic winds analyzed by low-pass objective analysis. In Figure 4, the reanalyzed oceanic winds are used to define the surface frontal boundary and to reveal the propagation of the surface cold front over the ocean north of Hawaii during 11-12 April 2008. At the descending time (0200-0400 UTC) 11 April, a distorted surface frontal boundary is determined by the wind shift and wind confluence (Fig. 4a), which is slightly ahead of the surface front subjectively analyzed in the surface weather map (Fig. 2a). In the postfrontal regions, the strong northwesterly flow (Fig. 4a) has a maximum around 15-17.5 m s^{-1}. At the ascending time (1300-1700 UTC) 11 April, the southern portion of the frontal boundary moves eastward and affects the Hawaii regime (Fig. 4b). Meanwhile, strong winds occur in the postfrontal regions and the wind speeds in the surrounding ocean of Hawaii also increase significantly. The frontal boundary moves eastward quickly over the ocean at the descending time of 12 April (Fig. 4c) and the wind increases in the Hawaiian Island chain, especially on land and over the nearby ocean north of Hawaii. The surface front subsequently moves outside the analyzed domain and dissipates.

.Improvement in the prediction of a Kona storm

At 0000 UTC on 5 April 2008, the surface weather map, subjectively analyzed by the Hawaii Forecasting Office (HFO), shows that a Kona low forms over the ocean northeast of Hawaii (Fig. 5a). A high-pressure center is located at the northwest of the Kona storm over the open ocean. Compared with the surface weather map, the satellite-derived ocean surface wind at the descending time (0200-0400 UTC) on 5 April 2008 reveals a significant cyclonic circulation (Fig. 5b) consistent with a low-pressure system there (Fig. 5a). Apparent wind speeds greater than 10 m s^{-1} are shown over the open ocean around the Kona low. Meanwhile, an anticyclonic circulation pattern (Fig. 5b) associated with a high-pressure system (Fig. 5a) located over the northwest of the Kona low, is also revealed from the retrieved oceanic winds, although there is a blank swath passing through the center of the anticyclonic circulation.

Through the incorporation of the satellite-derived ocean surface wind by the WRF 3D-Var system, the low-level winds at the 1000-hPa level (Fig. 6a) with assimilated oceanic wind obviously increase the northerly wind component over the Hawaiian islands and the nearby ocean, as compared with the global forecasting system (GFS) analysis

(Fig. 6b). The difference in the wind speed of the initial 1000-hPa winds reveals that a maxima center (> 4 m s^{-1}) occurs over the nearby ocean, just south of the Island of Oahu (Fig. 6c). Outside the Hawaiian Island chain, the impact of the assimilated oceanic wind is reduced over the ocean. In the vertical, the impact of the low-level winds can reach the 750-hPa level (not shown).

For the evolution of sea level pressure (SLP) associated with a Kona low during 5-7 April 2008, the NCEP reanalysis (Fig. 7) reveals that a significant decrease in the SLP of the Kona low from 1800 UTC 5 April to 0000 UTC 6 April, the low-pressure system then maintains its intensity over the open ocean northeast of Hawaii in the following day, but the quick drop (3hPa/6hr) in the SLP of the Kona low is not completely reproduced by the numerical predictions. However, the numerical prediction with assimilated oceanic winds (Fig. 7) is consistent with the NCEP reanalysis within the 18-hr simulations and improves the predicted SLP trend within the 36-hr simulations as compared with the GFS run and NCEP reanalysis. Recall that the Kona storm is a cold-core low and has its maxima intensity in the upper level. On the basis of the 48-hr 500-hPa cold-core temperature variation (Fig. 8), the NCEP reanalysis reveals that the obvious increase of the cold-core temperature before the quick deepening of the Kona low. The model simulations including assimilated oceanic winds and GFS run also reproduce the temperature-increased trend in the cold core, but the simulated temperature in the cold core increases more smoothly during the quick deepening period of the Kona low. In addition, the vertical cross sections in the difference of the temperature and geopotential-height variation related to the center of the Kona low during the first period (1800 UTC-1200 UTC 5 April, 2008) (Figs. 9a and 9b) and during the second period (0000 UTC 6 April-1800 UTC 5 April, 2008) (Figs. 9c and 9d) are analyzed. For the NCEP reanalysis, the significant environmental warming along the cold core of the Kona low at the first period occurs in the upper levels with the maxima (~3.5^{o}C) at the 300-hPa level (Fig. 9a). At the second period, the maxima warming (~3.5^{o}C) shifts to the middle level around the 500-hPa level (Fig. 9c). The low levels also have significant environmental warming associated with the Kona low. Meanwhile, the geopotential height reduces apparently in the low levels at the second period (Fig. 9d) compared with the first period (Fig. 9b). It indicates that the Kona low deepens significantly in the second period. For the numerical simulation with the assimilated oceanic winds (Fig. 10), the results at the first period also reproduce the environmental warming with the maxima (~2.5^{o}C) at the 300-hPa level (Fig. 10a), consistent with the NCEP reanalysis. At the second period, the significant middle level warming revealed by the NCEP reanalysis is not reproduced well through the Quik run, but the weaker environmental warming (Fig. 10c) and the decrease in the geopotential height (Fig. 10d) associated with the Kona low in the low levels are simulated. Furthermore, the results from the NCEP reanalysis (Fig. 11a) and the numerical simulation with assimilated oceanic winds (Fig. 11b) have a higher environmental warming as compared with GFS run at 0000 UTC 06 April 2008. These indicate that obvious environmental warming play an important role in the quick deepening of a Kona storm.

To investigate the associated mechanism for the environmental warming and the subsequent deepening of the Kona low, the latent heating effect due to the rainfall production and the environmental moisture content are further studied. Based on the IR satellite imageries during 1200 UTC 5 April-0000 UTC 6 April 2008 (Fig. 12), the

comma-like cloud pattern is revealed in the time slot of the quick deepening of the Kona storm. For the simulated 12-hr accumulated rainfall distribution during 1200 UTC 5 April-0000 UTC 6 April 2008 (Fig. 13a), the significant rainfall is reproduced over the ocean in the eastern part of the Kona storm and has the maxima around 40 mm, consistent with the TRMM 12-hr accumulated rainfall distribution (Fig. 13b). But the simulated rainfall maxima by the Quik and GFS runs only have half of the 12-hr accumulated rainfall amount retrieved by TRMM. The less simulated rainfall amount may imply that the less latent heating rate is reproduced in the numerical simulations. For the environmental moisture content at 1800 UTC 5 April prior to the quick deepening of the Kona low, the NCEP reanalysis (Fig. 14a) shows that a maximum precipitable water (PW) locates in the Kona low-pressure regime, consistent with the PW retrieved from SSM/I (Fig. 14b). For the difference in the PW between the NCEP reanalysis and the GFS run, the simulated PW by the GFS run (Fig. 14c) is less than the NCEP reanalysis.

Therefore, the numerical simulations by the assimilated oceanic winds (Quik run) and the GFS run reproduced less moisture content and less rainfall amount in the environment of the Kona storm. It implies that the weaker latent heating and weaker environmental warming is reproduced by the numerical predictions. These possibly lead to the weaker deepening in the predicted sea level pressure of the Kona low.

4. Conclusion

With the help of the satellite derived ocean surface wind from QuikSCAT satellite, the wind shift and wind confluence from the reanalyzed ocean surface winds can be utilized to determine the frontal boundary and reveal the propagation of a cold front over the open ocean, north of the Hawaiian Islands during 11-12 April 2008. Meanwhile, the strengthening of the northeasterly flow over Hawaii with the eastward-migrating high-pressure system is also revealed during the passage of the surface cold front.

The assimilated satellite-derived ocean-surface winds improve the cyclonic circulation of a Kona storm over the open ocean in the initial condition and also improve the prediction of the sea-level-pressure trend of the Kona low within the 36-hr forecasting as compared with the NCEP reanalysis and GFS run. But the quick deepening of the low-pressure center over the open ocean northeast of Hawaii during the 18-hr-24-hr forecasting can not be entirely captured. The 12-hr accumulated rainfall amount prior to the quick deepening of the Kona low predicted by the Quik and GFS run is less than that retrieved from TRMM. It implies that weaker latent heating is reproduced by the numerical predictions. Meanwhile, the predicted environmental warming in the middle and low levels during the same period is weaker than that revealed by the NCEP reanalysis. These possibly lead to the weaker deepening in the predicted sea level pressure of the Kona low after 18-hr simulation.

References

Atlas R.R., R. N. Hoffman, S.M. Leidner, J. Sienkiewicz, T. –W. Yu, S. C. Bloom, E. Brin, J. Ardizzone, J. Terry, D. Bungato, and J.C. Jusem, 2001: The effects of marine winds from scatterometer data on weather analysis and forecasting. *Bull. Amer. Meteorol. Soc*., **82**, 1965–1990.

Barker, D. M., W. Huang, Y.-R. Kuo, J. Bourgeois, and Q. Xiao, 2004: A three-dimensional variational data assimilation system for WRF-ARW: Implementation and initial results. *Mon. Wea. Rev.*, **132,** 897–914.

Maddox, R., 1980: An objective technique for separating macroscale and mesoscale features in meteorological data. *Mon. Wea. Rev.*, **108,** 1108–1121.

Skamarock W. C., J. B. Klemp, J. Dudhia, D. O. Gill, D. M. Barker, M. G. Duda, X. –Y Huang, W. Wang, J. G. Powers, 2008: A Description of the Advanced Research WRF Version 3, NCAR Technical Note, NCAR/TN-475+STR, 113pp.

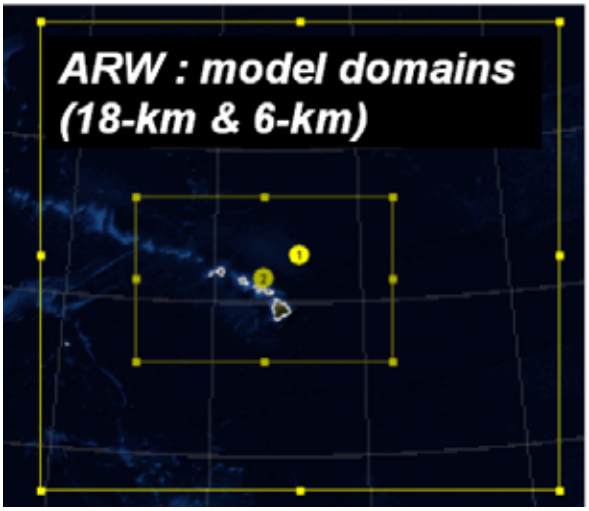

Fig. 1. Model domains with 18-km, and 6-km horizontal resolution for the course domain and nested domain.

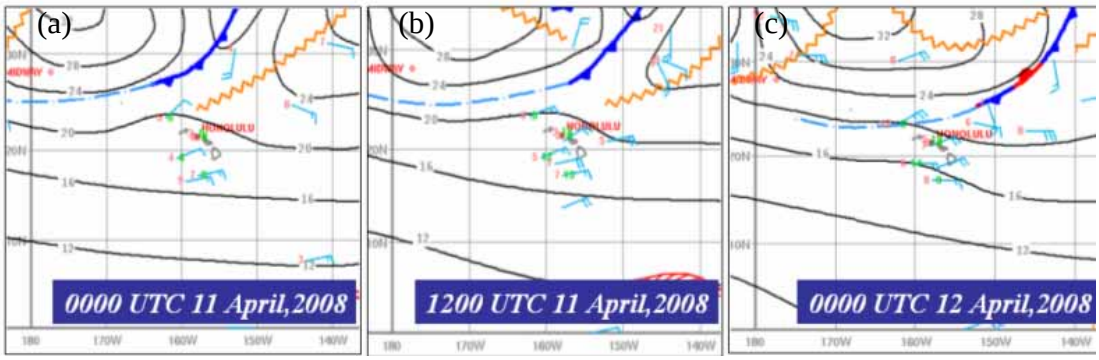

Fig. 2. Surface weather analysis by Hawaiian Forecasting Office (HFO) at (a) 0000 UTC on 11 April 2008, (b) 1200 UTC on 11 April 2008, and (c) 0000 UTC on 12 April 2008,

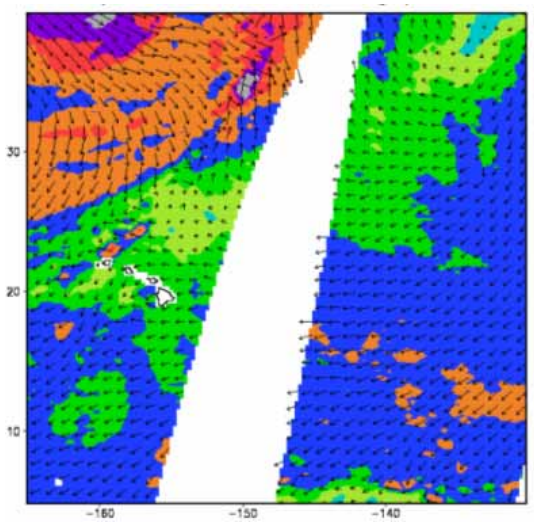

Fig. 3. The satellite-derived ocean surface winds at 0200-0400 UTC on 5 April 2008. The wind speed (color shaded) starts from 5 m s^{-1} with a 2.5 m s^{-1} interval.

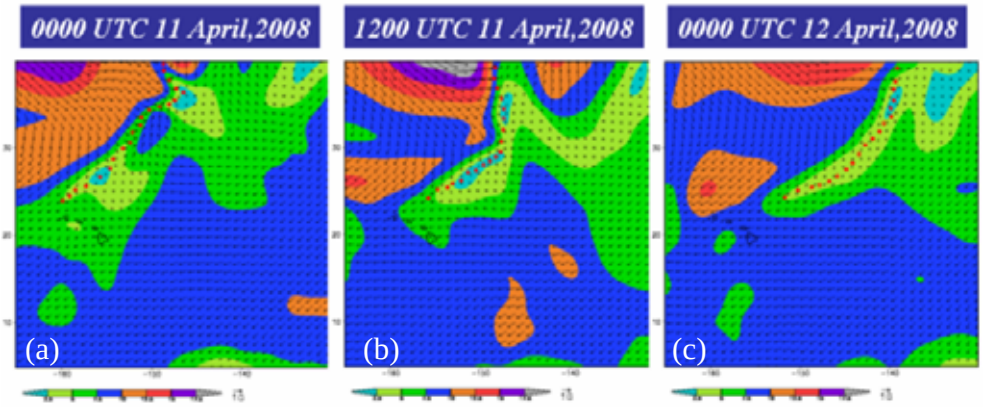

Fig. 4 The reanalyzed satellite-derived ocean surface winds at a) 0000 UTC on 11 April 2008, (b) 1200 UTC on 11 April 2008, and (c) 0000 UTC on 12 April 2008. The wind speed (color shaded) starts from 2.5 s^{-1} with a 2.5 m s^{-1} interval. Red dotted line represents the surface frontal boundary.

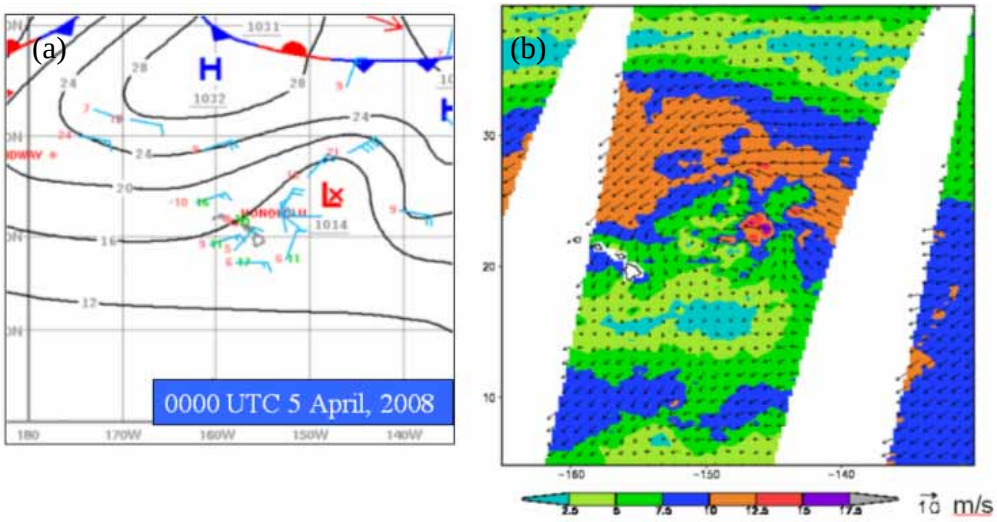

Fig. 5. (a) Surface weather analysis by Hawaiian Forecasting Office (HFO) at 0000 UTC on 5 April 2008, and (b) The satellite-derived ocean surface winds at 0200-0400 UTC on 5 April 2008. The wind speed (shaded) starts from 5 m s^{-1} with a 2.5 m s^{-1} interval.

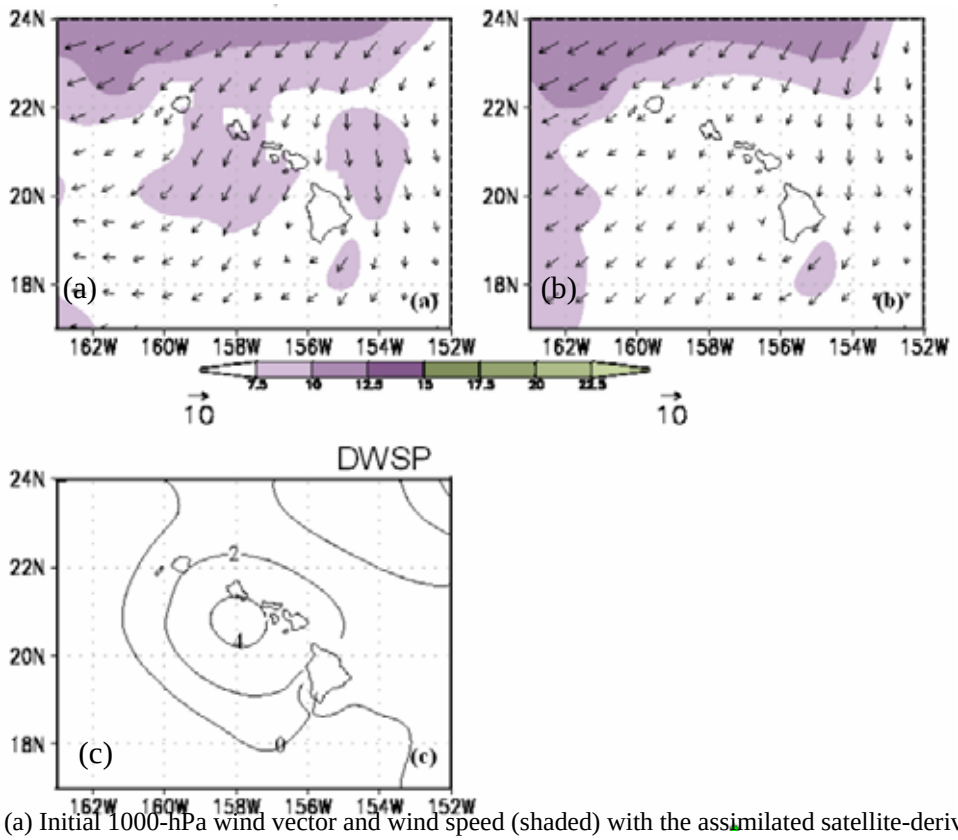

Fig. 6. (a) Initial 1000-hPa wind vector and wind speed (shaded) with the assimilated satellite-derived ocean surface winds, (b) Initial 1000-hPa wind vector and wind speed (shaded) for the GFS run, and (c) The contour of wind speed difference between (a) and (b) with a 2 m s^{-1} interval, at 0000 UTC 5 April 2008. The shaded in (a) and (b) starts from 5 m s^{-1} with a 2.5 m s^{-1} interval.

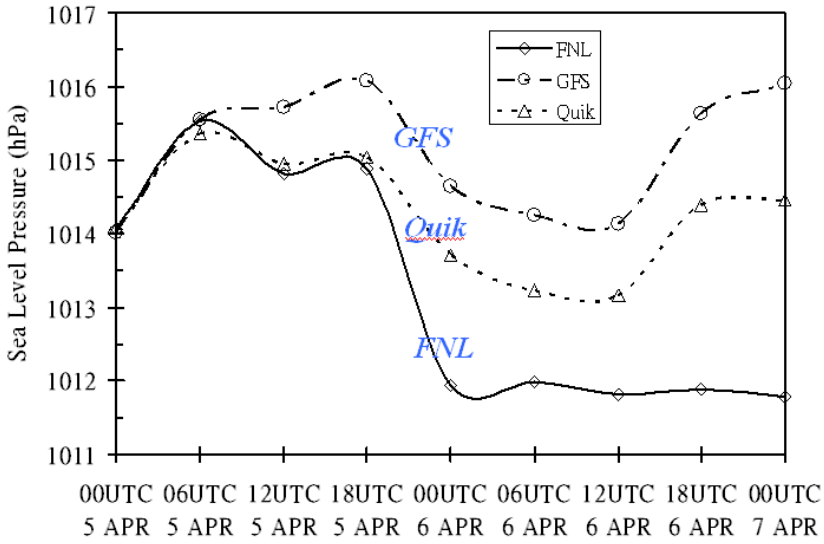

Fig. 7. Predicted 48-hr sea-level pressure by the Quik and GFS run, and the NCEP-fnl reanalysis.

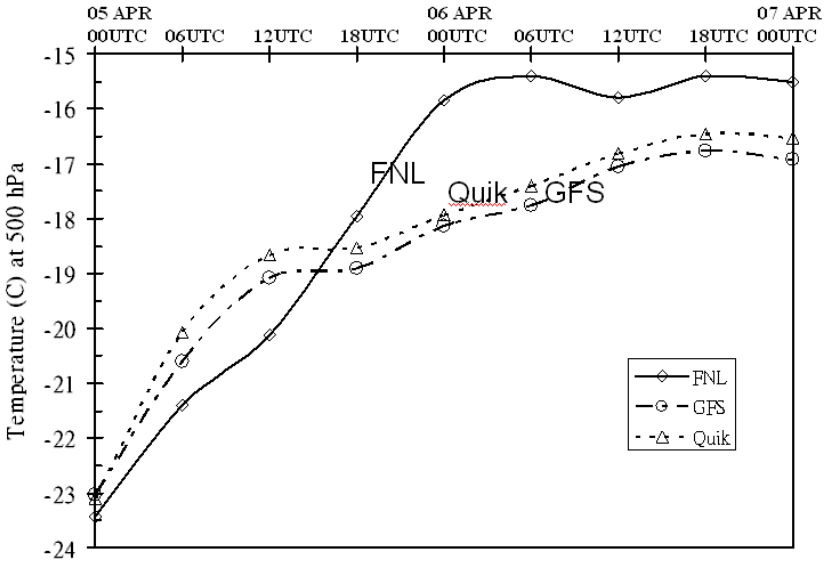

Fig. 8. Predicted 48-hr temperature at the cold core of the Kona low by the Quik and GFS run, and the NCEP-fnl reanalysis.

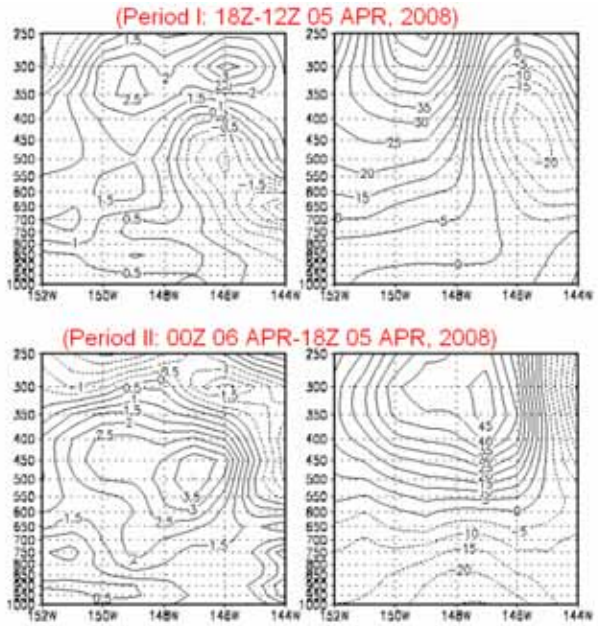

Fig. 9.The vertical cross-section of the temperature (left panel) and geo-potential height (right panel) differences during period I and period II using the NCEP reanalysis.

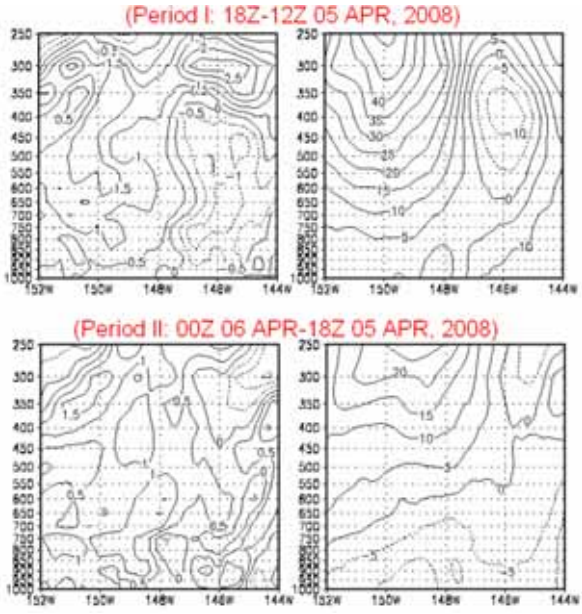

Fig. 10. Same as Figure 9 but for the Quik run.

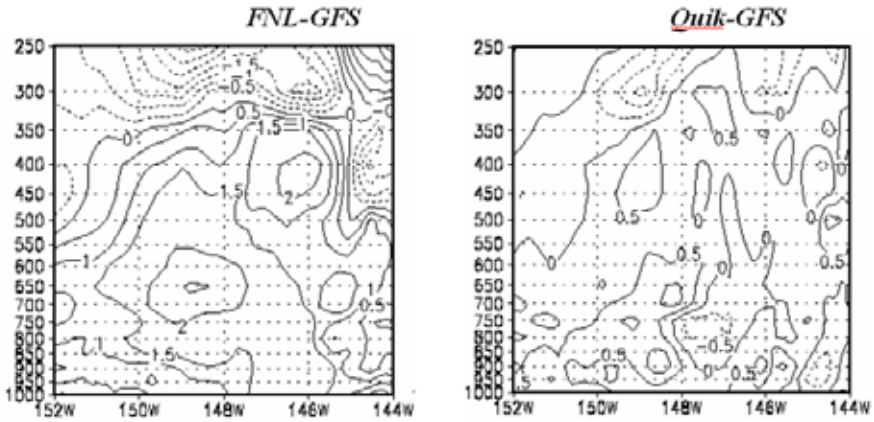

Fig. 11. Same as the Figure 9 but for the difference between the Quik and GFS run.

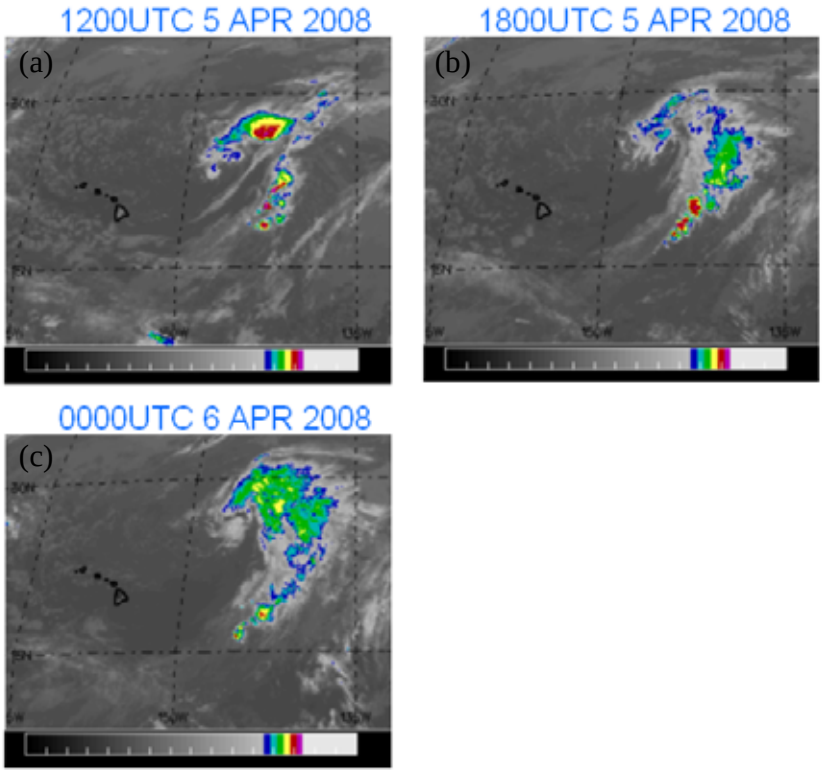

Fig. 12. Satellite imageries at (a) 1200 UTC 5 April, (b) 1800 UTC 5 April, and (c) 0000 UTC 6 April 2008.

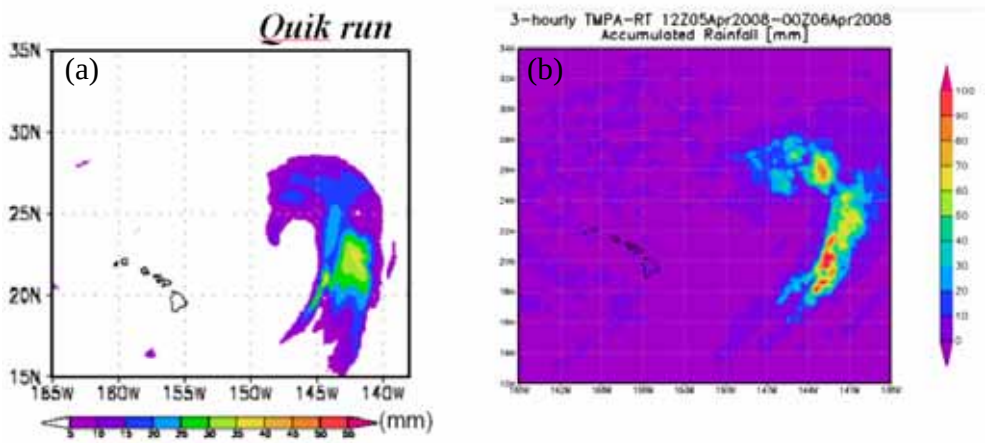

Fig. 13. (a) Simulated 12-hr accumulation rainfall by Quik run, and (b) Retrieved 12-hr accumulation rainfall from TRMM.

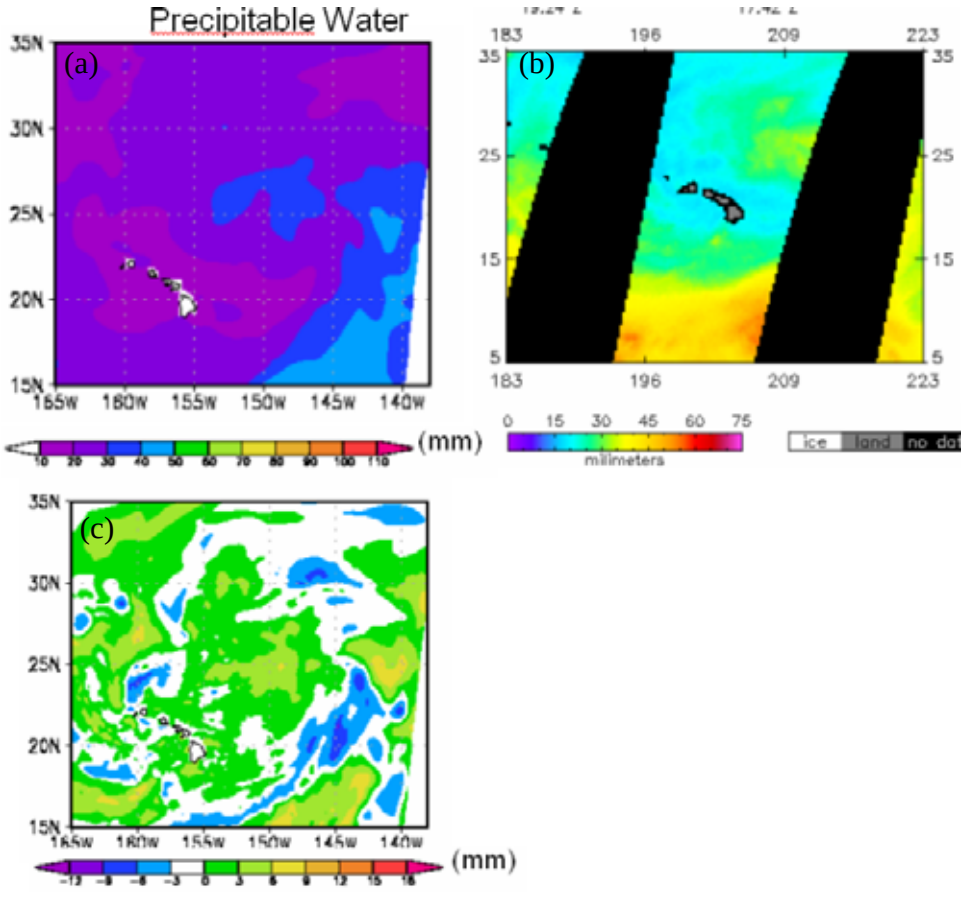

Fig. 14. (a) Precipitable water distribution from the NCEP reanalysis, (b) Precipitable water distribution from the SSM/I, and (c) Difference in the precipitable water between the NCEP reanalysis, and the GFS run at 1800 UTC 5 April 2008.